

## Article

# Supergene Hydrous Sulfates in the Tuolugou Co-Au Deposit, Northern Qinghai–Tibet Plateau: Implications for Genetic Mechanism and Exploration

Sida Niu <sup>1,2</sup> , Huaying Wu <sup>1,2,\*</sup>, Jianpeng Zhang <sup>3</sup>, Xianglong Niu <sup>1,2</sup>, Yingchao Wang <sup>1,2</sup>, Xiaoju Lin <sup>4</sup>, M. Santosh <sup>5,6</sup> and Jiahao Chen <sup>1,2</sup>

- <sup>1</sup> Institute of Mineral Resources Research, China Metallurgical Geology Bureau, Beijing 101300, China; niusida@cmgb.cn (S.N.)
  - <sup>2</sup> Mineral Comprehensive Utilization Research and Development Center, China Metallurgical Geology Bureau, Beijing 101300, China
  - <sup>3</sup> Qinghai Geological Exploration Institute of China Metallurgical Geology Bureau, Xining 810001, China
  - <sup>4</sup> CAS Key Laboratory of Mineralogy and Metallogeny, Guangdong Provincial Key Laboratory of Mineral Physics and Material, Guangzhou Institute of Geochemistry, Chinese Academy of Sciences, Guangzhou 510640, China
  - <sup>5</sup> School of Earth Science and Resources, China University of Geosciences, Beijing 100083, China
  - <sup>6</sup> Department of Earth Science, University of Adelaide, Adelaide 5005, Australia
- \* Correspondence: wuhuaying@cmgb.cn

**Abstract:** Supergene hydrous sulfate minerals form through the oxygenation and weathering of primary sulfides. In the Qinghai–Tibet Plateau region, with an alpine and dry environment, hydrous sulfate minerals oxidized from pyrite-bearing ore bodies provide important clues regarding the mineralization and environment. The Tuolugou sedimentary-exhalative (SEDEX) Co-Au deposit is located in the East Kunlun metallogenic belt of the northern Qinghai–Tibet Plateau in China. In the mining district, pyrite is the prevalent Co-hosting sulfide mineral, and is partially exposed on the surface to weathering and oxidation. Herein, we document the mineral assemblages in the supergene oxidation zone in the Tuolugou deposit, probe the genesis of supergene assemblage, and explore the implications for exploration. Three zones can be recognized in the oxidation zone of the Tuolugou deposit, including the outer zone (natrojarosite), intermediate zone (rozenite and aplowite), and inner zone (roemerite and melanterite). The mechanism of oxidation under aerobic and anaerobic conditions, as well as zoning with different oxidation degrees, are described in detail. Hydrous sulfates such as natrojarosite can be used as possible indicators of the exploration of albitite-related SEDEX deposit in this region.

**Keywords:** supergene; hydrous sulfates; Qinghai–Tibet Plateau; genetic mechanism; exploration indicator



**Citation:** Niu, S.; Wu, H.; Zhang, J.; Niu, X.; Wang, Y.; Lin, X.; Santosh, M.; Chen, J. Supergene Hydrous Sulfates in the Tuolugou Co-Au Deposit, Northern Qinghai–Tibet Plateau: Implications for Genetic Mechanism and Exploration. *Minerals* **2023**, *13*, 1198. <https://doi.org/10.3390/min13091198>

Academic Editors: Paul Alexandre, Zhenyu Chen and Fangyue Wang

Received: 30 July 2023

Revised: 7 September 2023

Accepted: 8 September 2023

Published: 13 September 2023



**Copyright:** © 2023 by the authors. Licensee MDPI, Basel, Switzerland. This article is an open access article distributed under the terms and conditions of the Creative Commons Attribution (CC BY) license (<https://creativecommons.org/licenses/by/4.0/>).

## 1. Introduction

Hydrated iron sulfate minerals are common supergene minerals in the weathering crust of sulfide deposits in arid and alpine regions. Aqueous sulfates are formed by the oxidation and weathering of primary sulfides, and metal oxidation zones usually serve as important prospecting markers for metal sulfide deposits [1,2]. The decomposition of primary sulfide minerals in the oxidation zone is accompanied by the migration and precipitation of elements, resulting in the emergence of characteristic sulfate and oxide mineral species in the oxidation zone [3]. Thus, their detailed study can provide important constraints on the secondary enrichment process of the ore deposits in plateaus with arid and alpine environments [2].

Previously, some studies have reported the  $^{40}\text{Ar}/^{39}\text{Ar}$  chronology, chemical analysis, X-ray diffraction, Mössbauer spectrum and other aspects of a series of sulfate minerals in

the oxidation zones of sulfide deposits in the Hongshan mining area in the northern East Tianshan Mountains of Xinjiang [1,4–6], addressing the mineralogy, genetic mechanism, and formation environment. Some studies have also focused on theoretical and experimental research on hydrous sulfate minerals. Chou et al. [7] studied the equilibrium system of sulfate under 0.1 MPa pressure and different humidity levels. The crystal chemistry of synthetic jarosite group minerals was studied by Basciano and Peterson [8]. Billon and Vieillard [9] evaluated the enthalpy changes in hydrous sulfate minerals from a thermodynamic point of view. In recent years, some hydrous sulfate minerals have also been discovered as new minerals. For example, Pekov et al. [10] reported hydrous sodium titanium sulfate in the oxidation zone of pyrite in the Alcaparrosa mine in Chile, and named it calamaite.

In addition to the theoretical constraints on the oxidation process of sulfide deposits, the oxidation zones of sulfide deposits also have certain economic value. The sulfate minerals can be directly used in the hydrometallurgical copper-smelting and acid-making industries [1]. Compared with the traditional acid-making method of roasting pyrite, it has the advantages of a beneficiation process and environmental protection. Both primary sulfides and their oxides are important sources of cobalt [11]. In addition, the preservation of sulfate minerals during the long oxidation process of primary sulfides is of great significance for the study of paleoclimate and paleogeographical environments [3,12]. The generation of reactive oxygen species (ROS)  $H_2O_2$  and  $OH^\cdot$  from pyrite in anaerobic environments played an important role in the evolution of early Earth [13,14]. The combination of two  $OH^\cdot$  can produce  $H_2O_2$  and, subsequently,  $O_2$ , constituting a potential pathway for oxygen generation and accumulation on early Earth [15].

Pyrite is a significant component of the global sulfur system and the most abundant sulfide on the Earth's surface [11]. The Tuolugou deposit was the first discovered mid-to-large scale deposit dominated by cobalt, with accompanying Au, in the East Kunlun orogenic belt of Qinghai in recent years [16]. A quartz albite sedimentary exhalative rock serves as the important prospecting indicator for cobalt ore bodies in the Tuolugou deposit, and an important signature for SEDEX deposits [17,18]. The oxidation zoning is well-developed in the Duangou ore section, Tuolugou deposit. The mineralogical study of the jarosite system is important for evaluating the oxidation zones of sulfide deposits and prospecting [2]. However, studies on hydrous sulfate in the oxidation zones of cobalt sulfide deposits are still very scarce.

Pyrite is the most widespread cobalt-bearing mineral in the Tuolugou deposit. The pyrite oxidation process is a significant part of the global sulfur cycle and has important environmental implications in the formation of acid mine wastewater and the oxidation and acidification of sediments [19–21]. The widespread presence of hydrous sulfate minerals is not only strong evidence for the existence of an acidic aqueous environment, but also provides clues for understanding the environment during the evolution of surface substances [22,23].

On the basis of field geological investigation and microscopic observation, combined with scanning electron microscopy (SEM), composition analysis, X-ray diffraction (XRD), Fourier transform infrared (FTIR), and X-ray photoelectron spectroscopy (XPS), we carried out a systematic study on the hydrous sulfate mineral assemblages developed in the Duangou section of the Tuolugou deposit in Qinghai–Tibet Plateau. We aimed to characterize the mineralogy and to understand the oxidation processes of primary sulfide minerals, the migration processes of elements, and their significance.

## 2. Geological Setting

The eastern Kunlun orogen, located in the northern margin of the Qinghai–Tibet plateau, to the south of Golmud City (Figure 1a,b), is one of the important components of the Central Orogenic Belt of China [24]. It has experienced a long and complex geodynamic evolution, including the formation and disruption of an ancient continent nucleus, the formation of an oceanic basalt plateau, Paleozoic to early Mesozoic orogenic processes, and intracontinental tectono-thermal events [25–28]. The intense tectonic–magmatic activities

resulted in large-scale Cu-Ni-Co-Au-Fe metallogenic metal mineralization in the eastern Kunlun orogen, termed as the eastern Kunlun metallogenic belt. There are more than 10 giant-/large-/medium-scale Cu (Ni-Co-Au-Fe) ore deposits occurring in the belt, including Xiarihamu, Zhongyou, Kendekeke, Galinge, Niukutou, Yemaquan, Shitoukengde, Langmuri, Dulenggou, Haisi, Xiaowolong, Shengli, Deerni [29], and Tuolugou, which are discussed in this paper.

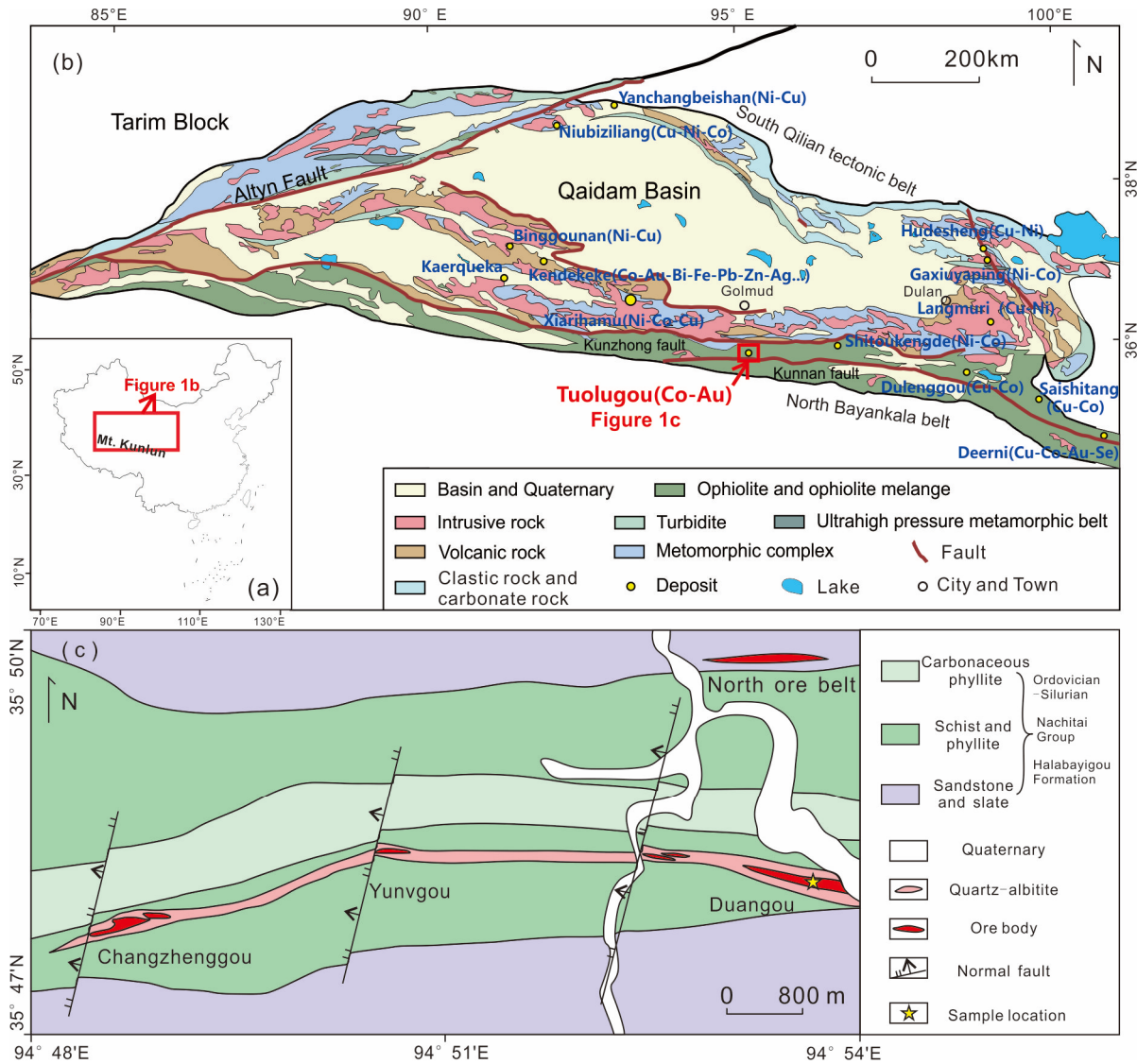


**Figure 1.** Geological background of the Tuolugou deposit. (a) Location and (b) regional geological setting of East Kunlun–Northern Qaidam region; (c) detailed geological map of the Tuolugou deposit (modified after [16]).

The Tuolugou Co-Au deposit, located between the Kunzhong and Kunnan faults (Figure 1b), is in the middle section of the Eastern Kunlun metallogenic belt. The Kunnan continental margin active belt is located between the Kunzhong fault and the Kunnan fault, with a length of about 1500 km from east to west and a width of about 60 km from north to south. The Caledonian period is generally characterized by continental crust extension, forming volcanic–sedimentary structures rich in cobalt, gold, and other metals. The Yanshanian–Himalayan period was characterized by south-to-north thrusting, resulting in deformation and mineralization in the area [16]. The strata in this region are mainly metamorphosed volcanic–sedimentary rock series. Meso-Neoproterozoic Wanbao-

gou Group, Ordovician–Silurian Nachitai Group, and Permian–Triassic marine–terrestrial sedimentary rocks are widely exposed. The magmatic activity in this region is weak, and intrusive rocks are barely exposed. The volcanic rocks are dominated by Ordovician–Silurian Nachitai Group Halabayigou Formation pyroclastic rocks. There are a number of shear zones trending EW and NW, along which cobalt, gold, copper, and other minerals are concentrated [16,18].

The overall strike is near east-west trending, with the north ore belt dipping south and the south ore belt dipping north. The exposed strata in the Tuolugou deposit are the Ordovician–Silurian Nachitai Group and Halabayigou Formation, which are composed of carbonaceous phyllite; shist and phyllite; and sandstone and slate, from old to new (Figure 1c). According to the different locations, the ore system can be divided into northern and southern blocks. The ore bodies controlled by the northern ore belt occur in sandstone and slate, while the ore bodies controlled by the southern ore block are found in schist and phyllite. The southern ore block includes the E-W trending Changzhenggou, Yunvgou, and Duangou deposits, from east to west. The east-west-trending folds in Tuolugou are dominated by the Gounao syncline. The area shows well-developed schistosity as part of the regional tectonic activity [18].

### 3. Sampling and Analytical Methods

#### 3.1. Field Sampling

The samples from the Tuolugou deposit were collected from the Duangou ore section, where there is a well-developed oxidation belt. Representative samples were collected from the different zones (location shown in Figures 1c and 2, detailed information displayed in Table 1). The center of the oxidation belt shows an isomorphism of cobalt in pyrite. The pyrite displays a faint yellow color, whereas it is brassy yellow when exposed to weathering. The wall rock consists of quartz albitite and phyllite. The oxidation zone in the surface is rather unconsolidated, with a sulfuric smell.

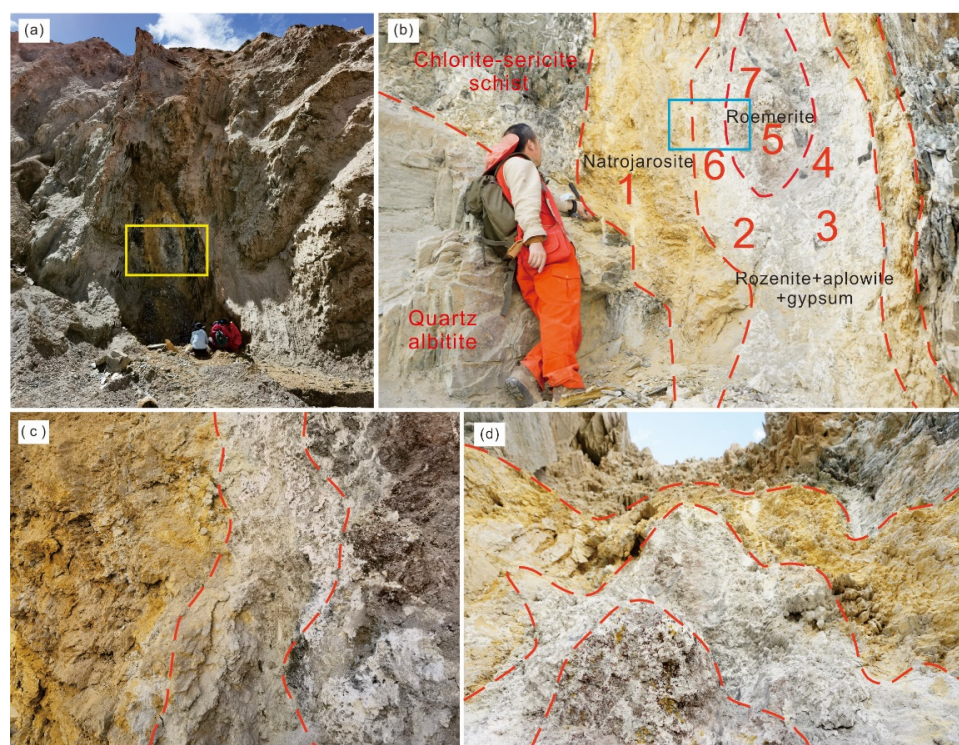


**Figure 2.** Outcrop of the hydrous sulfate zoning from the Duangou ore section, Tuolugou deposit. (a) Location of Figure 2b; (b–d) zoning of the oxidation zone. Numbers in Figure 2b indicate the sampling locations of Sample 3-1 to Sample 3-7.

**Table 1.** Sampling information of the supergene hydrous sulfate assemblage of the Duangou ore section, the Tuolugou deposit.

	Sample No.	Color	XRD Test Method	Main Mineral Phases
Outer zone	DG3-1	Earthy yellow	Powder XRD	Quartz, albite, natrojarosite
Intermediate zone	DG3-2	Pale pink	Powder XRD	Rozenite, apowite
	DG3-3	Ashy		Rozenite, pyrite, szomolnokite
	DG3-4	Absinthe-yellow		Rozenite, gypsum, sulfur
	DG3-6	Off-white		Rozenite, gypsum, muscovite
Inner zone	DG3-5	Crimson	Powder and single-crystal XRD	Pyrite, quartz, gypsum, romerite
	DG3-7	Charcoal grey/Wathet blue		Pyrite, rozenite, melanterite

### 3.2. Analytical Methods

The 60–80 mesh samples collected from the oxidation zone of the Tuolugou deposit were pasted onto conductive adhesive for scanning electron microscopy (SEM) and energy dispersive spectroscopy (EDS) analysis. The SEM and EDS analyses were carried out in the Electron Probe Laboratory of the Key Laboratory of Mineral Resources Research, Chinese Academy of Sciences, using a ZEISS GeminiSEM 450 SEM and OXFORD ULTIM MAX spectrometer.

X-ray diffraction was performed at the Institute of Science, China University of Geosciences (Beijing). A Rigaku Smart lab 9000 W X-ray powder crystal diffractometer (rotating target, post-graphite monochromator) was used for the powder XRD with a Cu K $\alpha$  radiation source. For powder XRD, the conditions were 40 kV and 200 mA, and X-ray diffraction patterns were collected at 3–70° (2 $\theta$ ) with a scanning rate of 0.02° (2 $\theta$ ) s<sup>−1</sup>. Single-crystal X-ray powder diffraction was carried out using a Bruker D2 Phaser X-ray diffractometer with a Cu K $\alpha$  radiation source. X-ray diffraction patterns were collected between 5 and 80° (2 $\theta$ ) at a scanning rate of 1° (2 $\theta$ ) min<sup>−1</sup> ( $\lambda$  = 0.154 nm, 30 kV, 10 mA). The Le Bail routine (Peakfit) and manually picked peaks were combined for XRD indexing. The Rietveld method with extraction of the structure factors (Fobs) was used to refine the unit cell parameters.

The semiquantitative composition analysis was determined using a Japan Rigaku ZSX Primus II X-ray fluorescence spectrometer at Northwestern University. The detection range was F and later elements, without calibrating loss on ignition. The spectra in the mid-infrared range (approximately 4000–400 cm<sup>−1</sup>) for the samples were collected using a Bruker VERTEX 70 Fourier transform infrared (FTIR) spectrometer at Guangdong Provincial Key Laboratory of Mineral Physics and Materials, Guangzhou, China. The spectra were obtained in transmission (can be converted to absorbance) mode. The spectra were collected in the 400 to 4000 cm<sup>−1</sup> (with KBr beam splitter) range with a spectral resolution of 0.5 cm<sup>−1</sup>. All the samples were embedded in KCl pellets and analyzed in the absorbance mode. The samples were pressed using pressure in the range of 55 to 60 kb, followed by the recording of the spectra. The surface element compositions and chemical environments were analyzed using Thermo Fisher K-Alpha X-ray photoelectron spectroscopy (XPS).

## 4. Mineralogical Characterization

In this work, through field observation and stereoscopic observation, combined with XRF (X-ray Fluorescence) major element analysis and single crystal and powder crystal XRD work, the hydrous sulfate minerals in the alteration zone of the Duangou ore section, Tuolugou deposit, were identified and characterized.

Natrojarosite NaFe<sub>3</sub>[SO<sub>4</sub>]<sub>2</sub>(OH)<sub>6</sub>, trigonal occurs in the outer zone, with a light-yellow to brown color, as the coating of albite and quartz (Figure 3a). The quartz albitite is weathered, with micron-sized natrojarosite crystals developed on the surface, individual grains of 1–3  $\mu$ m, and small crystals agglomerating to form sparse clumps of 3–10  $\mu$ m.

Rozenite FeSO<sub>4</sub>•4(H<sub>2</sub>O), which is monoclinic, occurs as a tender, earthy, whitish powder covering the oxidation surface of the ore body, and also as a powdery product of the dehydration of melanterite (Figure 3b).

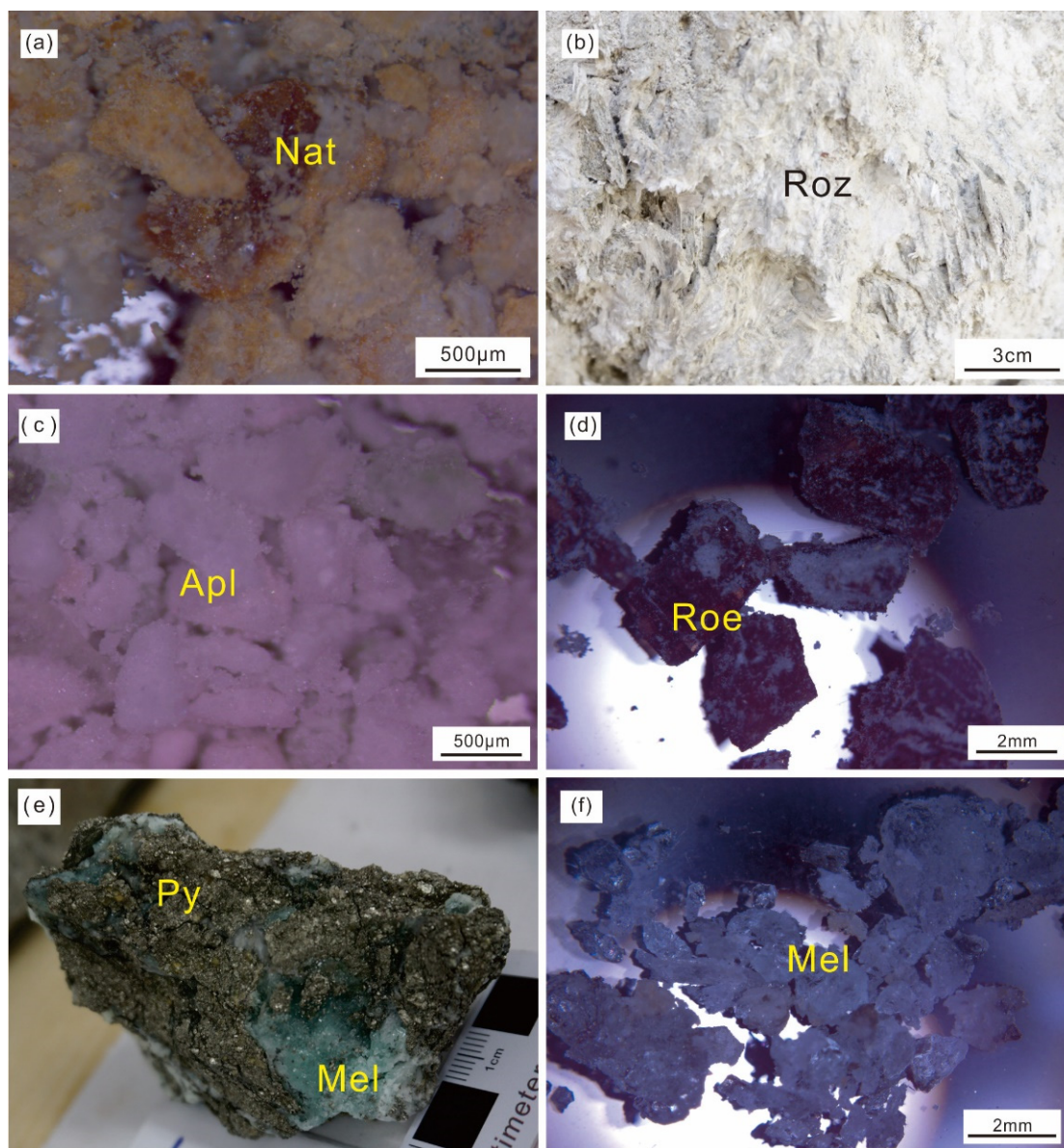


**Figure 3.** Typical stereoscopic microphotographs of the samples from the oxidation zone of the Duangou ore section, Tuolugou deposit. (a) Natrojarosite; (b) rozenite; (c) aplowite; (d) roemerite; (e) pyrite and melanterite; (f) melanterite. Nat—natrojarosite; Roz—rozenite; Apl—aplowite; Roe—roemerite; Py—pyrite; Mel—melanterite.

Aplowite  $\text{CoSO}_4 \cdot 4(\text{H}_2\text{O})$  is a monoclinic, cyclic cobalt sulfate tetrahydrate. It is fine-coarse granular, pink, and vitreous (Figure 3c), which is diagnostic indicator of the supergene of cobalt deposits.

Roemerite  $\text{FeFe}_2\text{SO}_4 \cdot 14(\text{H}_2\text{O})$ , is triclinic and idiomorphic, with single crystals 1–5 mm in size, a maroon-ocher-brown color, complete crystal output, and vitreous luster (Figure 3d).

Melanterite  $\text{FeSO}_4 \cdot 7(\text{H}_2\text{O})$ , is monoclinic, granular or fibrous, and light green-blue, with a silky luster and masses in its aggregates (Figure 3e,f). Melanterite is found in association with roemerite.

In addition to pyrite and hydrous sulfate minerals, minerals such as gypsum, mica, and quartz are also developed in the alteration zone. Roemerite and melanterite were recognized by single-crystal XRD. Natrojarosite, rozenite and aplowite were identified by powder XRD. Few of the mineral phases were confined to sulfate accumulation and could not be identified reliably by powder XRD due to their small size and sporadic occurrence.

## 5. Results

Micrometer-scale mineral particles are recognized under SEM-EDS, as indicated in Figure 4. Albite, natrojarosite, aplowite, native sulfur, rozenite, roemerite, pyrite, and melanterite are recognized as crystals of euhedral micron grade. Powder XRD results of the samples are shown in Figure 5. Sample DG3-1 was characterized by natrojarosite, DG3-2, DG3-3, DG3-4 and DG3-6 by rozenite. Pyrite was the diagnostic mineral phase in samples DG3-5 and DG3-7. Major elements identified by XRF are shown in Figure 6.  $\text{SO}_3$  (with an average of 45.7 wt.%),  $\text{Fe}_2\text{O}_3$  (with an average of 31.8 wt.%),  $\text{SiO}_2$  (with an average of 11.0 wt.%),  $\text{Al}_2\text{O}_3$  (with an average of 5.4 wt.%),  $\text{K}_2\text{O}$  (with an average of 1.7 wt.%), and  $\text{CaO}$  (with an average of 1.5 wt.%) are the oxides that averaged more than 1 wt.% of the seven samples (Table 2). Following these are  $\text{Co}_2\text{O}_3$ ,  $\text{MgO}$ ,  $\text{As}_2\text{O}_3$ ,  $\text{TiO}_2$ ,  $\text{NiO}$ ,  $\text{P}_2\text{O}_5$ , and  $\text{Na}_2\text{O}$ , of which the average values were less than 1 wt.%. The content of  $\text{Co}_2\text{O}_3$  ranged between 0.12 and 1.09 wt.%, with an average of 0.46 wt.%. The cell parameters of roemerite and melanterite are shown in the cif files as Supplementary Materials.

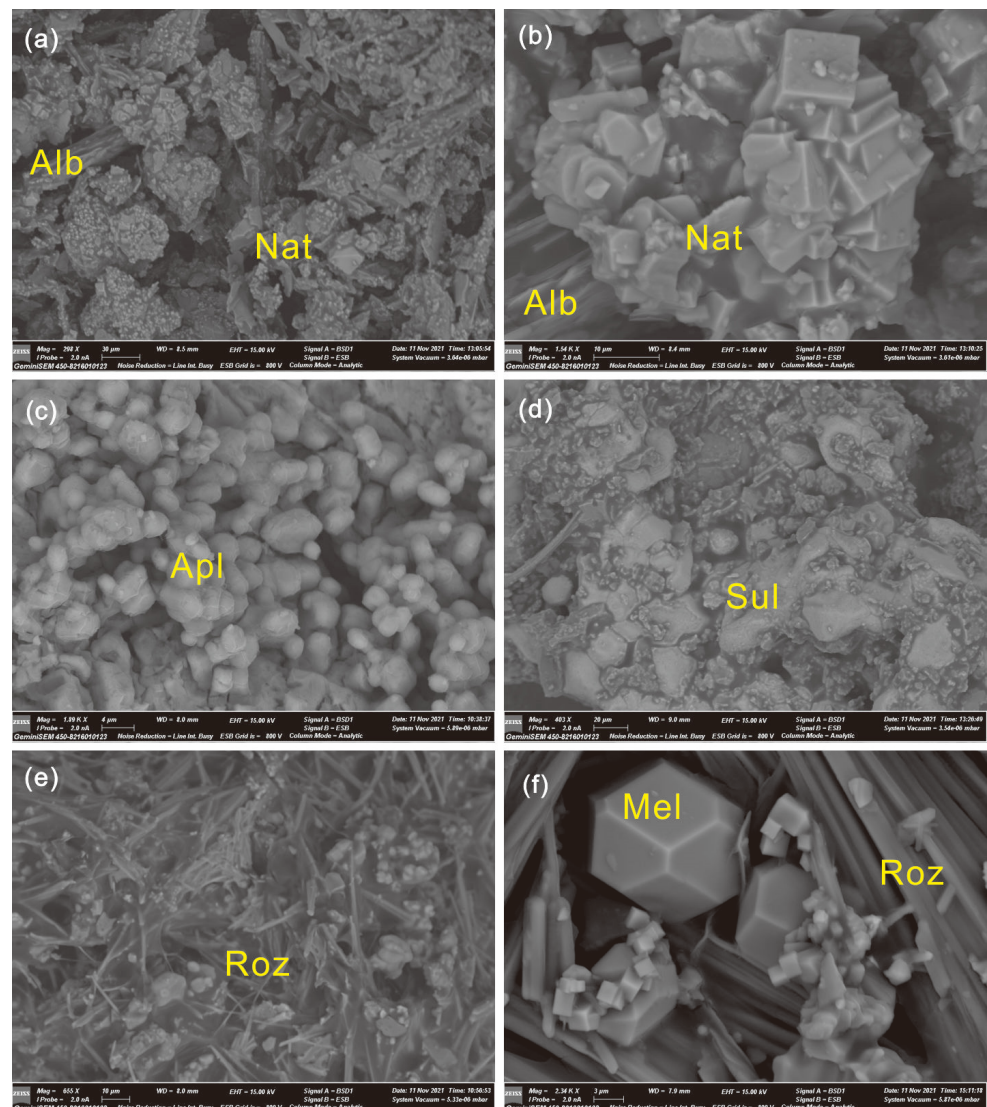


**Figure 4.** Typical SEM microphotographs of the samples from the oxidation zone of Duangou ore section, Tuolugou deposit. (a,b) Natrojarosite and albite; (c) aplowite; (d) native sulfur; (e) rozenite; (f) melanterite and rozenite. Alb—albite; Nat—natrojarosite; Apl—aplowite; Sul—native sulfur; Roz—rozenite; Roe—roemerite; Py—pyrite; Mel—melanterite.

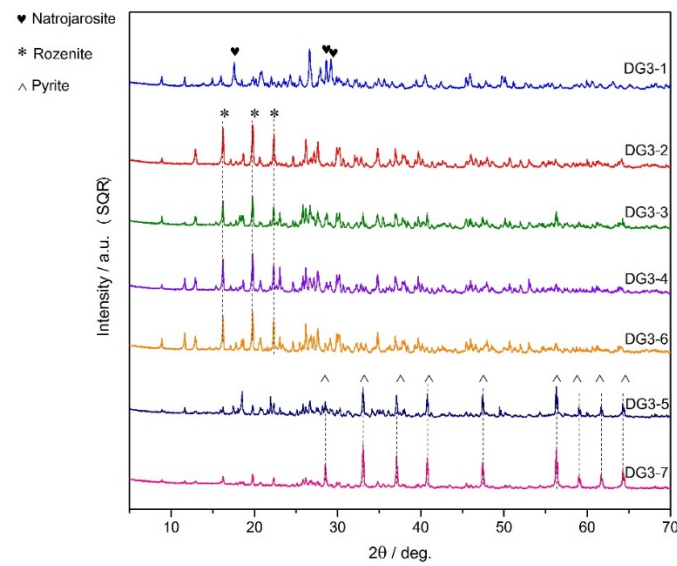


**Figure 5.** X-ray powder diffraction patterns of the samples from the oxidation zone of Duangou ore section, Tuolugou deposit.

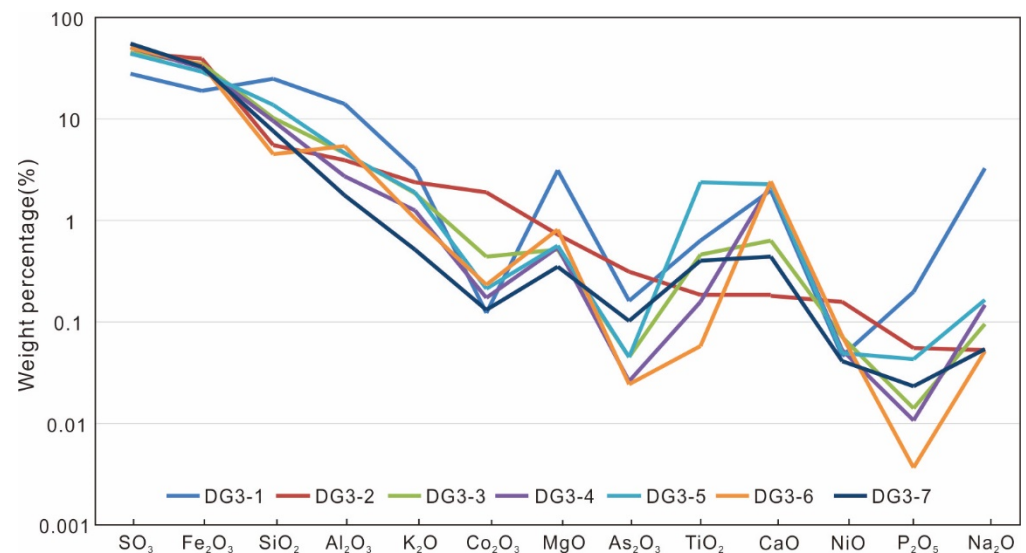


**Figure 6.** Major element composition of the samples from the oxidation zone of Duangou ore section, Tuolugou deposit.

**Table 2.** Chemical composition of the samples from the oxidation belt of the Tuolugou Co(Au) deposit from XRF (wt.%).

	SO <sub>3</sub>	Fe <sub>2</sub> O <sub>3</sub>	SiO <sub>2</sub>	Al <sub>2</sub> O <sub>3</sub>	K <sub>2</sub> O	Co <sub>2</sub> O <sub>3</sub>	MgO	As <sub>2</sub> O <sub>3</sub>	TiO <sub>2</sub>	CaO	NiO	P <sub>2</sub> O <sub>5</sub>	Na <sub>2</sub> O
DG3-1	27.92	19.16	25.17	14.30	3.22	0.12	3.15	0.16	0.63	2.01	0.05	0.20	3.27
DG3-2	45.09	39.41	5.55	3.97	2.37	1.90	0.73	0.31	0.18	0.18	0.16	0.06	0.05
DG3-3	45.55	35.28	10.33	4.59	1.88	0.45	0.52	0.04	0.47	0.64	0.07	0.01	0.10
DG3-4	50.48	32.43	9.60	2.77	1.26	0.17	0.54	0.03	0.16	2.26	0.05	0.01	0.15
DG3-5	44.26	29.33	13.92	4.63	1.88	0.22	0.56	0.05	2.37	2.27	0.05	0.04	0.17
DG3-6	50.57	34.61	4.58	5.45	1.05	0.24	0.81	0.02	0.06	2.43	0.07	0.00	0.05
DG3-7	55.97	32.53	7.61	1.80	0.52	0.13	0.35	0.10	0.41	0.44	0.04	0.02	0.05
Average	45.69	31.82	10.96	5.36	1.74	0.46	0.95	0.10	0.61	1.46	0.07	0.05	0.55

The XPS results are shown in Figure 7 and Table 3. For the outer zone (Sample DG3-1), sulfur of the +4 valence was predominant. For the intermediate zone, minor S<sup>2+</sup> could be

detected, whereas  $S^{2+}$  was abundant in the inner zone. The Fe XPS results show various valences on the surfaces of the samples from the oxidation zone of the Tuolugou deposit. Sulfide and sulfate occupied different proportions in different zones. For the outer zone,  $Fe^{3+}$  was predominant, and in the intermediate zone,  $Fe^{2+}$  and  $Fe^{3+}$  in oxidation products comprised the majority of the samples.  $Fe^{2+}$  in sulfide represented a nonnegligible part of the inner zone. The FT-IR results are presented in Figure 8 and Table 4. All of the samples showed broad bands of water molecules and valleys of about  $1620\text{--}1640\text{ cm}^{-1}$  of water. The  $SO_4^{2-}$  also showed shoulders of about  $3350\text{--}3400\text{ cm}^{-1}$  and  $1000\text{--}1150\text{ cm}^{-1}$ . Three zones were recognized in the oxidation zone of the Duangou ore section, Tuolugou deposit, as shown in Figure 2, and the details are discussed in Section 6.2.

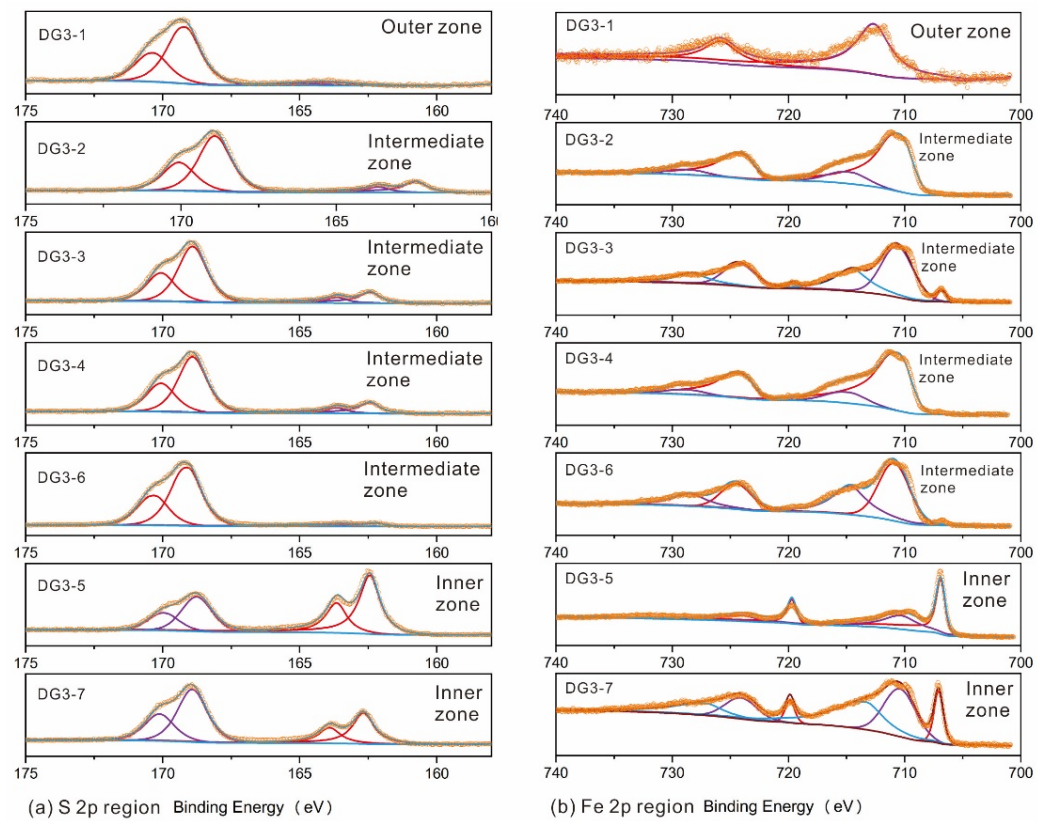


**Figure 7.** X-ray photoelectron spectroscopy spectra (XPS) of the samples from the oxidation zone of Duangou ore section, Tuolugou deposit, in the S2p and Fe2p regions. The purple, red, and blue lines are the fitting curves of the elements with different valence states. The orange circles are the measured XPS data.

**Table 3.** The Gauss fitting results of the Fe2p and S2p XPS spectra.

Sample	$Fe^{3+}$		$Fe^{2+}$ sulfate		$Fe^{2+}$ sulfide		$S^{4+}$		$S^{2+}$		
	Peak/eV	Area/%	Peak/eV	Area/%	Peak/eV	Area/%	Peak/eV	Area/%	Peak/eV	Area/%	
Outer zone	DG3-1	712.66	100.0					169.19	88.47	163.88	11.53
Intermediate zone	DG3-2	714.72	16.22	710.43	83.78			169.03	100.0		
	DG3-3	714.53	33.57	710.62	62.83	706.79	3.60	168.91	79.35	162.42	20.65
	DG3-4	714.89	14.60	710.54	85.40			169.12	88.90	163.63	11.10
	DG3-6	714.72	39.02	710.90	60.98			169.09	89.11	162.21	10.89
Inner zone	DG3-5			710.34	45.01	706.91	54.99	168.76	37.66	162.44	62.34
	DG3-7	713.33	45.90	710.40	40.57	707.07	13.53	168.92	76.11	163.90	23.89

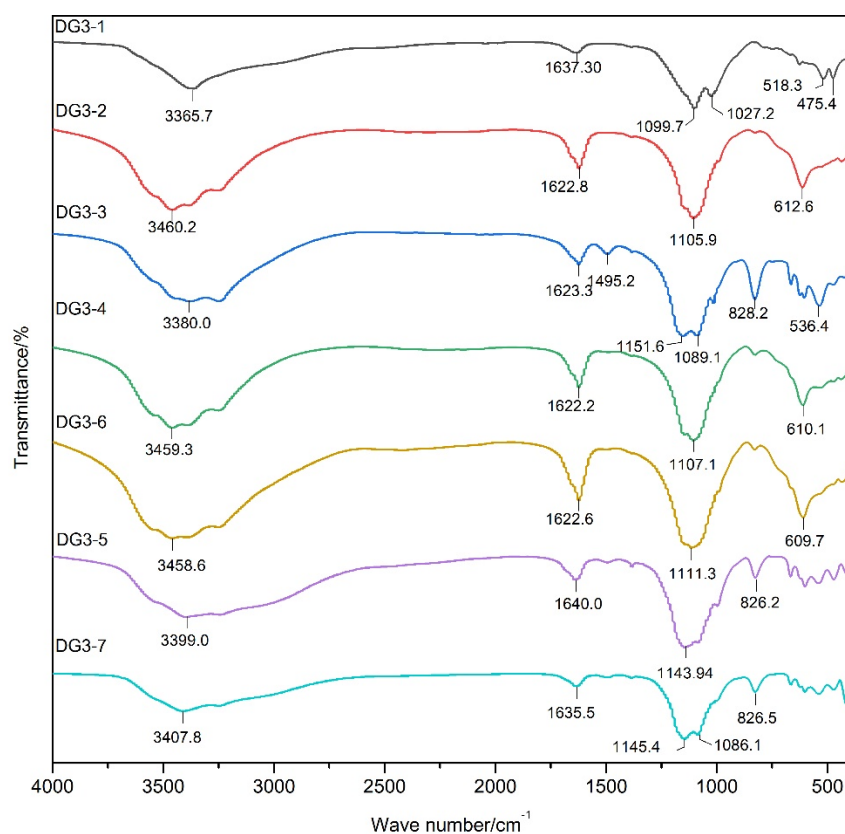


**Figure 8.** Fourier transform infrared spectroscopy spectra of the samples from the oxidation zone of Duangou ore section, Tuolugou deposit.

**Table 4.** Absorbance peak assignments and peak positions for the sample ( $\text{cm}^{-1}$ ) of the FTIR spectrum for the samples from the Duangou section, Tuolugou deposit.

	Sample No.	Symmetrical Stretching Mode of $\text{SO}_4^{2-}$	Asymmetrical Stretching Mode of $\text{SO}_4^{2-}$	Bending Mode of $\text{H}_2\text{O}$	Stretching Mode of $\text{H}_2\text{O}$ and $\text{OH}^-$
Outer zone	DG3-1	518.3, 475.4	1099.7, 1027.2	1637.3	3365.7
	DG3-2	612.6	1105.9	1622.8	3460.2
Intermediate zone	DG3-3	536.4, 828.2	1151.6, 1089.1	1623.3	3380.0
	DG3-4	610.1	1107.1	1622.2	3459.3
	DG3-6	609.7	1111.3	1622.6	3458.6
Inner zone	DG3-5	826.2	1143.9	1640.0	3399.0
	DG3-7	826.5	1145.4, 1086.1	1635.5	3407.8

## 6. Discussion

### 6.1. Genesis of Supergene Sulfate Assemblage

Different types of sulfates have been recognized from metal and coal mines worldwide, including jarosite, natrojarosite, melanterite, rozenite, etc. [8]. Dry and cold climates are beneficial for the preservation of the hydrous sulfate as the oxidation product of the ore bodies. The hydrous sulfates are often accompanied by sulfur and goethite [30]. Oxidation of pyrite is the most ubiquitous in metallic ore deposits. The oxidation of pyrite is recognized as:  $2\text{FeS}_2 + 7\text{O}_2 + 2\text{H}_2\text{O} \rightarrow 2\text{Fe}^{2+} + 4\text{H}^+ + 4\text{SO}_4^{2-}$  [2].  $\text{Fe}^{3+}$  can further promote the formation of acidic water as an oxidant and help to release other metal ions into the water [31].  $\text{Fe}^{2+}$

can be easily oxidized into Fe<sup>3+</sup> on the surface. Fe<sup>3+</sup> can become the oxidant and catalyst in the process of the oxidation of FeS<sub>2</sub>, forming hydrous sulfate minerals [32].

Hydrous iron sulfate minerals have been found in other arid region deposits in China, which is considered as an intuitive indicator for deep mineralization [1,2]. The Tuolugou deposit in northern Qinghai–Tibet Plateau is a SEDEX deposit with pyrite as the main Co-containing mineral [33]. As for the oxidation zone in this deposit, various hydrous iron sulfate minerals can be found, including natrojarosite, rozenite, roemerite, and melanterite. Cobalt, in the oxidation zone, occurs as a hydrous Co sulfate—aplowite—in this deposit (Figure 3c). The aplowite represents the diagnostic supergene mineral of Co mineralization.

Quartz albitite is an important host rock of Co-bearing pyrite in the Tuolugou deposit, generally occurring in layered or quasi-layered form, and forms rhythmic laminae with sericite quartz schist and chlorite sericite quartz schist [16,33]. The weathering and fragmentation of quartz albitite are accompanied by the migration and precipitation of Na ions from albitite, which provides a sufficient source of Na ions for the formation of natrojarosite. The formation of hydrous sulfate requires water, oxidation, and an acidic environment. Therefore, natrojarosite can be used as an indicative mineral in the oxidized zone of the Tuolugou deposit in arid regions.

The pyrite–water interface generates reactive oxygen species (including hydroxyl radicals, hydrogen peroxide, etc.) which can produce oxidation reactions at relatively deep depths [32,34,35]. Under the function of strong solar radiation and evaporation, and in an arid climate, supergene sulfate minerals appear. In the Na-rich Tuolugou deposit, the characteristic natrojarosite appears.

### 6.2. Mechanism of Oxidation and Zoning

According to the field observation and mineral assemblages, three zones can be recognized in the oxidation zone, namely, the outer zone, intermediate zone, and inner zone (Figures 2 and 9, Table 3).

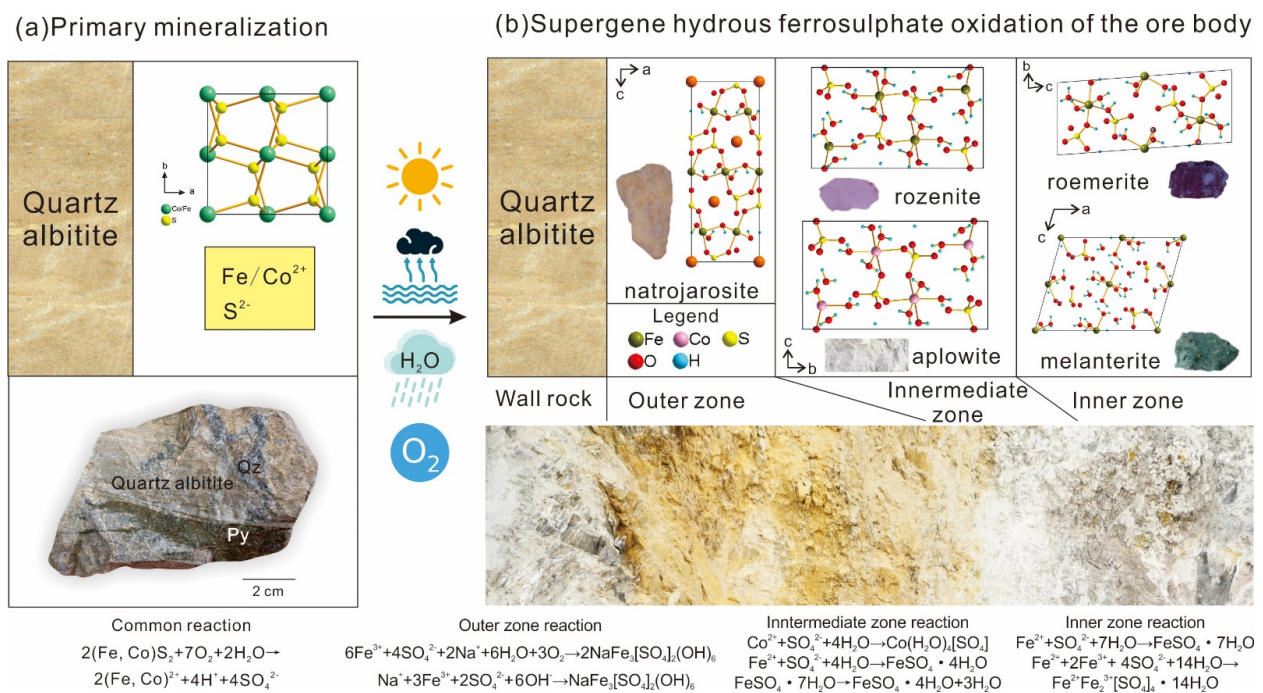


**Figure 9.** (a) Primary sulfides. (b) Precipitation of secondary sulfate minerals by myriad processes like oxidation, hydrolysis, and evaporation.

Outer zone (Sample DG3-1): On the margin of the quartz albitite, which is yellow-light brown, the weathering product occurs as micron-sized natrojarosite. Fe mainly appears as +3 valence.

Intermediate zone (Samples DG3-2, DG3-3, DG3-4, DG3-6): Rozenite and aplowite appeared, white-rose pink, characterized by a hydrous cobalt sulfate. Fe presents as a mix of +3 and +2 valence.

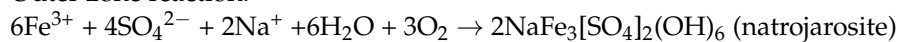
Inner zone (Sample DG3-5, DG3-7): Millimeter-sized roemerite and melanterite crystal could be observed. Roemerite was maroon to dark red, while melanterite was light blue to green. In general, Fe<sup>+2</sup> made up the majority of the Fe element in this zone. Pyrite plays an important role in the inner zone, and it was restored under the surface of the supergene.

The sample DG3-5 and DG3-7 showed wider peaks of water in the FT-IR graphs (Figure 8), suggesting a stronger association of the hydrogen bond from the outer zone to the inner zone [36]. From the outer zone to the inner zone, the unit cell became bigger, the symmetry degree became lower, and more water entered the crystal structure (Figure 8). The difference might be attributed to the activity of a Co-bearing pyrite ore body with water and oxygen. The inner zone has a high proportion of pyrite, which has the highest reactivity and can produce reactive oxygen even under oxygen-free conditions [35], accompanied by a complex structure and strong hydrogen bonding of the conjoining effect. The valence of Fe increases from the inner zone to outer zone, suggesting a high oxidation degree of the outer zone.

Sulfur was found in sample DG3-4 very rarely, as a microscopic admixture in the sulfate accumulation at sites 2 and 4. It formed 50 to 75 mm-sized crystals that sat on the sulfate. Under the electron beam, the crystals tended to melt rapidly. Sulfur can be considered as an intermediate product of the oxidation of pyrite [3]. In summary, the oxidation route of pyrite in air to form hydrous sulfate is described below.

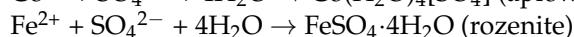
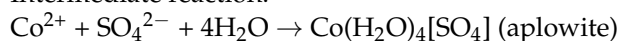
Fe and Co occur as isomorphisms in primary pyrite ores, but they separated in oxide ores. A common reaction was  $2(\text{Fe, Co})\text{S}_2 + 7\text{O}_2 + 2\text{H}_2\text{O} \rightarrow 2(\text{Fe, Co})^{2+} + 4\text{H}^+ + 4\text{SO}_4^{2-}$ . Under the condition of insufficient oxidation, part of the iron in ferrous sulfate will become ferric iron.

Outer zone reaction:



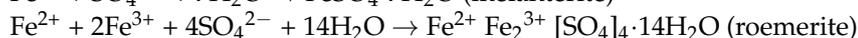
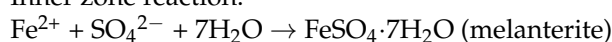
$\text{Na}^+ + 3\text{Fe}^{3+} + 2\text{SO}_4^{2-} + 6(\text{OH})^- \rightarrow \text{NaFe}_3[\text{SO}_4]_2(\text{OH})_6$  (natrojarosite hydroxyl radicals in hydroxylation on pyrite from anaerobic environment)

Intermediate reaction:



$\text{FeSO}_4 \cdot 7\text{H}_2\text{O} \rightarrow \text{FeSO}_4 \cdot 4\text{H}_2\text{O} + 3\text{H}_2\text{O}$  (dehydration of melanterite to form rozenite under dry environment)

Inner zone reaction:



### 6.3. Implications on Exploration

The geological, geophysical, and geochemical indicators are summarized below. The metallogenic age is Ordovician, and a hydrothermal sedimentary basin is an advantageous tectonic environment. Halabayigou Formation, Nachitai Group is the primary ore-bearing stratum. The geophysical marker is an anomaly of high polarization and low resistance, or high polarization and high resistance. The abnormal distribution area of Co in 1:50,000 drainage anomalies measured by stream sediment can be regarded as the geochemical indicator [37]. The weathering and crushing of quartz albitite, which is characteristic of Na-rich SEDEX deposits, is accompanied by the precipitation of Na ions [17,33]. The formation of natrojarosite requires water, oxidation, and an acidic environment, while the soluble nature of natrojarosite indicates that its preservation requires an arid environment [38]. The strong sunlight and short precipitation time in the plateau, with very limited water infiltration into the subsurface, often cause the cobalt ore body media to maintain a small amount of water and high acidity. Moreover, sulfate minerals are soluble, which makes them able to be preserved only in arid areas. During the oxidation process, some of the iron and cobalt

migrate from the primary cobalt ore body to the oxidation zone. Therefore, cobalt-bearing natrojarosite can be used as an indicator mineral in the oxidation zone of SEDEX deposits in arid regions, providing clues for the exploration of cobalt polymetallic deposits in arid regions of the plateau. Certain hydrous ferrosulfate minerals can be regarded as indicators of exploration on a plateau or in an analogous environment. Aplowite can be considered as a direct clue for cobalt mineralization on a plateau.

The Tuolugou deposit is not being exploited at present, and oxidized zones are exposed on the surface. Zoning of hydrous iron sulfate assemblages is a direct clue for Co mineralization in plateau or arid conditions, especially when (1) Co > 0.1 wt.% in the oxidation sample; (2) Co sulfate appears. Other favorable indicators include (1) high percentage of +2 valence of Fe; (2) wild H<sub>2</sub>O peak in 3500 cm<sup>-1</sup>; (3) sophisticated crystal structure/higher percentage of water. Co-bearing pentagonal dodecahedron pyrite in the ore body is sensitive to oxidation, and it has greater reaction activity and speed as well as more oxygen and water [32,34,35]. Thus, the detailed study of hydrous sulfate can provide insights into the exploration of cobalt–polymetallic deposits on plateaus and areas with similar arid climates.

## 7. Conclusions

This study evaluates the oxidation mechanism of cobalt-bearing pyrite in the Tuolugou deposit on the Qinghai–Tibet Plateau, where various types of hydrous ferrosulfates occur. Certain assemblages of hydrous sulfate can be considered as indicators of ore deposits. Natrojarosite can be used as a possible indicator for the exploration of Na-rich SEDEX deposits.

Based on the study of the genesis of supergene hydrous sulfate and oxidation mechanisms, the formation model of oxidation zonation was established. Three zones were identified in the oxidation zone of the Tuolugou deposit, including the outer zone (natrojarosite), intermediate zone (rozenite and aplowite), and inner zone (roemerite and melanterite). The valence of iron varied from +3 to +2 from the outer zone to the inner zone, with more water involved and a more complex crystal structure.

Potential prospecting indicators for cobalt polymetallic deposits in arid and semi-arid regions of the plateau are proposed. Oxidation indicators of mineralization lead to the following inferences: (1) high percentage of +2 valence of Fe; (2) hydrous sulfate with strong association of the hydrogen bond; (3) hydrous sulfate with superior unit cell.

## 8. Patents

This achievement has been submitted to the State Intellectual Property Office of the People's Republic of China for an invention patent called "A mineralogical prospecting method for cobalt polymetallic deposits in arid and semi-arid areas of plateau". The application number is: 202211661644.6.

**Supplementary Materials:** The following are available online at <https://www.mdpi.com/article/10.3390/min13091198/s1>, the cif files of roemerite and melanterite.

**Author Contributions:** S.N. prepared the manuscript; H.W. provided supervision and instructions for the article; J.Z. and X.N. provided help with the fieldwork and investigation, and also gave important insights on the discussion; Y.W. supported the sample collection and analysis. X.L. supported the XPS and FT-IR experiments; M.S. reviewed and edited the manuscript; J.C. helped to collect the samples and provide important documents on geology. All authors have read and agreed to the published version of the manuscript.

**Funding:** This research was funded by the second comprehensive scientific investigation of the Qinghai–Tibet Plateau (Grant No. 2019QZKK0801) and the Science and Technology Planning Project of Guangdong Province, China (Grant No. 2020B1212060055).

**Data Availability Statement:** Some data presented in this study are included within the article and Supplementary Materials. Other data are available upon request from the corresponding author, Huaying Wu.

**Acknowledgments:** Shenglong Bai, Jun Wang, Bingfei Yu, and Tong Pan are sincerely thanked for their help during field work. Guangyao Liu, Lingchao Mo, Haiyang Xian, Guowu Li, and Lin Li are sincerely thanked for their patient help.

**Conflicts of Interest:** The authors declare no conflict of interest.

## References

1. Qin, K.Z.; Ding, K.S.; Xu, Y.X.; Miao, Y.; Fang, T.H.; Xu, X.W. Tremendous crystal-Paracoquimbite and its polytypecoquimbite found for the first time in Hongshan Hs-epithermal Cu-Au deposit, eastern Tianshan, NW-China, and its significance. *Acta Petrol. Sin.* **2008**, *24*, 1112–1122. (In Chinese with English Abstract).
2. Zhao, Z.; Zhao, Z. Sulphate supergene minerals: An intuitive indicator for deep deposit in plateau regions. *Geol. J.* **2021**, *56*, 4063–4079.
3. Matysek, D.; Jirásek, J.; Osovsky, M.; Skupien, P. Minerals formed by the weathering of sulfides in mines of the Czech part of the upper Silesian basin. *Mineral. Mag.* **2014**, *78*, 1265–1286.
4. Xu, Y.X.; Qin, K.Z.; Ding, K.S.; Li, J.X.; Miao, Y.; Fang, T.H.; Xu, X.W.; Li, D.M.; Luo, X.Q. Geochronology evidence of Mesozoic metallogenesis and Cenozoic oxidation at Hongshan HS-epithermal Cu-Au deposit, Kalatage region, eastern Tianshan, and its tectonic and paleoclimatic significances. *Acta Petrol. Sin.* **2008**, *24*, 2371–2383. (In Chinese with English Abstract).
5. Li, G.W.; Xiong, M.; Ding, K.S.; Qin, K.Z.; Xu, Y.X.; Fang, T.H. A New Superstructure in Copiapite. *Acta Mineral. Sin.* **2010**, *30*, 1–8. (In Chinese with English Abstract).
6. Guo, H.T.; Xu, Y.X.; Qin, K.Z. M(o)ssbauer Spectra Characteristics of Eight Sulfate Minerals in Oxidization Zone of Hongshan Hs-Epithermal Cu-Au Deposit, Eastern Tianshan, NW China, and Their Geological Significance. *Geol. Explor.* **2014**, *50*, 486–493. (In Chinese with English Abstract).
7. Chou, I.M.; Seal, R.R.; Hemingway, B.S. Determination of Melanterite-Rozenite and Chalcantite-BonattiteEquilibria by Humidity Measurements at 0.1 MPa. *Am. Mineral.* **2002**, *87*, 108–114. [[CrossRef](#)]
8. Basciano, L.C.; Peterson, R.C. Crystal chemistry of the natrojarosite-jarosite and natrojarosite-hydrionium jarosite solid-solution series: A synthetic study with full Fe site occupancy. *Am. Mineral.* **2008**, *93*, 853–862.
9. Billon, S.; Vieillard, P. Prediction of enthalpies of formation of hydrous sulfates. *Am. Mineral.* **2015**, *100*, 615–627. [[CrossRef](#)]
10. Pekov, I.V.; Siidra, O.I.; Chukanov, N.V.; Yapaskurt, V.O.; Belakovskiy, D.I.; Turchkova, A.G.; Möhn, G. Calamaite, a new natural titanium sulfate from the Alcaparrosa mine, Calama, Antofagasta region, Chile. *Eur. J. Mineral.* **2018**, *30*, 801–809. [[CrossRef](#)]
11. Hazen, R.M.; Hystad, G.; Golden, J.J.; Hummer, D.R.; Liu, C.; Downs, R.T.; Morrison, S.M.; Ralph, J.; Grew, E.S. Cobalt mineral ecology. *Am. Mineral.* **2017**, *102*, 108–116. [[CrossRef](#)]
12. Paramanick, S.; Rajesh, V.J.; Praveen, M.N.; Sajinkumar, K.S.; Bhattacharya, S. Spectral and chemical characterization of copiapite and rozenite from Padinjarathara in Wayanad, Southern India: Possible implications for mars exploration. *Chem. Geol.* **2021**, *575*, 120043. [[CrossRef](#)]
13. Blankenship, R.E.; Hartman, H. The origin and evolution of oxygenic photosynthesis. *Trends Biochem. Sci.* **1998**, *23*, 94–97. [[CrossRef](#)] [[PubMed](#)]
14. Schoonen, M.; Smirnov, A.; Cohn, C. A Perspective on the role of minerals in prebiotic synthesis. *AMBIO A J. Hum. Environ.* **2004**, *33*, 539–551. [[CrossRef](#)]
15. Borda, M.J.; Elsetinow, A.R.; Schoonen, M.A.; Strongin, D.R. Pyrite-Induced Hydrogen peroxide formation as a driving force in the evolution of photosynthetic organisms on an early earth. *Astrobiology* **2001**, *1*, 283–288. [[CrossRef](#)]
16. Feng, C.; Qu, W.; Zhang, D.; Dang, X.; Du, A.; Li, D.; She, H. Re-Os dating of pyrite from the Tuolugou stratabound Co(Au) deposit, eastern Kunlun Orogenic Belt, northwestern China. *Ore Geol. Rev.* **2009**, *36*, 213–220.
17. Ma, G.; Beaudoin, G.; Qi, S.; Ying, L. Geology and geochemistry of the Changba SEDEX Pb-Zn deposit, Qinling orogenic belt, China. *Miner. Deposita* **2004**, *39*, 380–395. [[CrossRef](#)]
18. Feng, C.; Qi, F.; Zhang, D.; Li, D.; She, H. China's first independent cobalt deposit and its metallogenic mechanism: Evidence from fluid inclusions and isotopic geochemistry. *Acta Geol. Sin.* **2011**, *85*, 1403–1418.
19. Hurtgen, M.T. The marine sulfur cycle, revisited. *Science* **2012**, *337*, 305–306. [[CrossRef](#)]
20. Ouyang, Y.T.; Liu, Y.; Zhu, R.L.; Ge, F.; Xu, T.Y.; Luo, Z.; Liang, L.B. Pyrite oxidation inhibition by organosilane coatings for acid mine drainage control. *Miner. Eng.* **2015**, *72*, 57–64. [[CrossRef](#)]
21. Rickard, D.; Mussmann, M.; Steadman, J.A. Sedimentary sulfides. *Elements* **2017**, *13*, 117–122. [[CrossRef](#)]
22. Liu, C.; Ling, Z.; Cao, F.; Chen, J. Comparative Raman and visible near-infrared spectroscopic studied of jarosite endmember mixtures and solid solutions relevant to Mars. *J. Raman Spectrosc.* **2017**, *48*, 1676–1684. [[CrossRef](#)]
23. Mckay, C.P. Prerequisites to human activity on mars: Scientific and ethical aspects. *Theol. Sci.* **2019**, *17*, 317–323. [[CrossRef](#)]
24. Dong, Y.P.; He, D.F.; Sun, S.S.; Liu, X.M.; Zhou, X.H.; Zhang, F.F.; Yang, Z.; Cheng, B.; Zhao, G.C.; Li, J.H. Subduction and accretionary tectonics of the East Kunlun orogen, western segment of the Central China Orogenic System. *Earth-Sci. Rev.* **2018**, *186*, 231–261. [[CrossRef](#)]
25. Xu, Z.; Yang, J.; Jiang, M.; Li, H.; Xue, G.; Yuan, X.; Qian, H. Deep structure and lithospheric shear faults in the East Kunlun-Qiangtang region, northern Tibetan Plateau. *Sci. China Ser. D* **2001**, *44*, 1–9. [[CrossRef](#)]

26. Song, S.G.; Bi, H.Z.; Qi, S.S.; Yang, L.M.; Allen, M.B.; Niu, Y.L.; Su, L.; Li, W.F. HP–UHP Metamorphic belt in the East Kunlun orogen: Final closure of the Proto-Tethys ocean and formation of the Pan-North-China Continent. *J. Petrol.* **2018**, *59*, 2043–2060. [[CrossRef](#)]
27. Wang, P.; Zhao, G.C.; Liu, Q.; Yao, J.L.; Han, Y.G. Evolution of the Paleo-Tethys Ocean in Eastern Kunlun, North Tibetan Plateau: From continental rift-drift to final closure. *Lithos* **2022**, *422–423*, 106717. [[CrossRef](#)]
28. Yu, M.; Dick, J.M.; Feng, C.Y.; Li, B.; Wang, H. The tectonic evolution of the East Kunlun Orogen, northern Tibetan Plateau: A critical review with an integrated geodynamic model. *J. Asian Earth Sci.* **2020**, *191*, 104168. [[CrossRef](#)]
29. Chen, J.; Wu, H.; Niu, X.; Niu, S.; Wang, Y.; Wang, J.; Wang, Z. Geology and geochronology of the Lalingzaohuo cobalt-bearing copper polymetallic skarn deposit, East Kunlun. *Ore Geol. Rev.* **2023**, *154*, 105349. [[CrossRef](#)]
30. Łukasz, K. Supergene sulphate minerals from the burning coal mining dumps in the Upper Silesian Coal Basin, South Poland. *Int. J. Coal Geol.* **2013**, *105*, 91–109.
31. Boon, M. The mechanism of direct and indirect bacterial oxidation of sulphide minerals. *Hydrometallurgy* **2001**, *62*, 67–70. [[CrossRef](#)]
32. Zhu, J.X.; Xian, H.Y.; Lin, X.J.; Tang, H.M.; Du, R.X.; Yang, Y.P.; Zhu, R.L.; Liang, X.L.; Wei, J.M.; Teng, H.H.; et al. Surface structure-dependent pyrite oxidation in relatively dry and moist air: Implications for the reaction mechanism and sulfur evolution. *Geochim. Cosmochim. Acta* **2018**, *228*, 259–274. [[CrossRef](#)]
33. Niu, S.D.; Wu, H.Y.; Niu, X.L.; Wang, Y.C.; Bai, S.L.; Chen, J.H.; Zhang, M.; Mo, L.C. Recognition of natrojarosite in Tuolugou Co (Au) deposit in middle-east section of East Kunlun Metallogenic Belt and its significance. *Miner. Depos.* **2022**, *41*, 1232–1244, (In Chinese with English Abstract).
34. Xian, H.Y.; Du, R.X.; Zhu, J.X.; Chen, M.; Tan, W.; Zhu, R.L.; Wei, J.M.; He, H.P. Hydration induced bandgap shift at pyrite-water interface. *Appl. Phys. Lett.* **2018**, *113*, 123901. [[CrossRef](#)]
35. Xian, H.Y.; Zhu, J.X.; Tan, W.; Tang, H.M.; Liu, P.; Zhu, R.L.; Liang, X.L.; Wei, J.M.; He, H.P.; Teng, H.H. The mechanism of defect induced hydroxylation on pyrite surfaces and implications for hydroxyl radical generation in prebiotic chemistry. *Geochim. Cosmochim. Acta* **2019**, *244*, 163–172. [[CrossRef](#)]
36. Bakker, D.J.; Peters, A.; Yatsyna, Y.; Zhaunerchyk, V.; Anouk, M.R. Infrared Signatures of Hydrogen Bonding in Phenol Derivatives. *J. Phys. Chem. Lett.* **2016**, *7*, 1238–1243. [[CrossRef](#)]
37. Kui, M.J.; Zhang, A.K.; Liu, Y.L.; Liu, Z.G.; He, S.Y.; Zhang, J.P.; Li, Z.F. The geological characteristics and prospecting mode of Tuolugou cobalt deposit, Qinghai. *Miner. Explor.* **2019**, *10*, 57–64, (In Chinese with English Abstract).
38. Blasco, M.; Gázquez, M.J.; Pérez-Moreno, S.M.; Grande, J.A.; Valente, T.; Santisteban, M.; Torre, M.L.; Bolívar, J.P. Polonium behaviour in reservoirs potentially affected by acid mine drainage (AMD) in the Iberian Pyrite Belt (SW Spain). *J. Environ. Radioact.* **2016**, *152*, 60–69. [[CrossRef](#)]

**Disclaimer/Publisher’s Note:** The statements, opinions and data contained in all publications are solely those of the individual author(s) and contributor(s) and not of MDPI and/or the editor(s). MDPI and/or the editor(s) disclaim responsibility for any injury to people or property resulting from any ideas, methods, instructions or products referred to in the content.